THE ASTROPHYSICAL JOURNAL, 481:433–446, 1997 May 20

OBSERVATIONS OF THE SW SEXTANTIS STAR BH LYNCIS IN A HIGH STATE

D. W. HOARD AND PAULA SZKODY
Department of Astronomy, University of Washington, Box 351580, Seattle, WA 98195-1580;
hoard@astro.washington.edu, szkody@astro.washington.edu
Received 1996 September 17; accepted 1996 December 18

ABSTRACT

We present time-resolved photometry and medium resolution (2 Å) spectroscopy of the SW Sextantis star BH Lyncis obtained during a high state of the system. Previous detailed observations have been obtained only during low and intermediate states. In addition, we present the first *International Ultraviolet Explorer* low-resolution (6 Å) spectrum of BH Lyn. A revised photometric ephemeris, HJD(min) = 2,447,180.3366(2) + 0.15587535(6)E, is derived based on new and previously published eclipse timings. The amplitude of the pre-eclipse hump in light curves of BH Lyn is shown to vary, suggesting that the degree to which the incoming accretion stream impacts the edge of the disk changes over time. We estimate system parameters using the V-band eclipse width and He II λ4686 emission-line radial velocity ($i \approx 79°$, $q \approx 0.45$, $M_{WD} \approx 0.7\ M_\odot$, $M_2 \approx 0.3\ M_\odot$, $R_2 \approx 0.4\ R_\odot$, $a \approx 1.2\ R_\odot$). Doppler tomograms constructed for the prominent emission lines in BH Lyn show a lack of emission at the expected locations of the bright spot and accretion stream trajectories. The differences between the low and high states of BH Lyn are discussed, along with the possible origin of a significant amount of the emission-line flux in a wind from the disk and/or white dwarf primary star. Finally, a model involving the presence of vertically extended bulges in the accretion disk is introduced to explain the characteristic phase-dependent absorption feature found in emission lines of the SW Sex stars.

Subject headings: accretion, accretion disks — binaries: close — novae, cataclysmic variables — stars: individual (BH Lyncis)

1. INTRODUCTION

The *SW Sex stars* denote a somewhat loosely defined subclass of cataclysmic variables (CVs) that share a number of observational characteristics. These dozen or so systems are all nova-like CVs; that is, they display photometric properties indicative of a high mass transfer rate greater than the critical level above which dwarf nova outbursts do not occur (Shafter 1992). They are typically high inclination systems ($i \gtrsim 80°$) that display prominent eclipses, but at least two CVs displaying characteristics of the SW Sex stars (WX Arietis and PG 0859+415; see Beuermann et al. 1992 and Hoard & Szkody 1996, respectively) appear to be of more moderate inclination ($i \lesssim 70°$). Further, they have orbital periods in the range 3–4 hr, just above the 2–3 hr period gap thought to result from the evolutionary transition from angular momentum loss primarily via magnetic braking of the secondary star ($P_{orb} > 3$ hr) to loss via gravitational radiation ($P_{orb} < 2$ hr), which suggests a possible evolutionary link to the onset of the SW Sex phenomenon.[1]

The SW Sex stars also display a number of unusual characteristics that set them apart from other CVs, such as (1) velocity curves of the emission lines that imply nonuniform emission from the accretion disk; (2) single-peaked emission lines in contrast to the expected double-peaked lines typically observed in high inclination disk systems; (3) the Balmer and He I lines have orbital-phase–dependent profiles characterized by the appearance of a strong central absorption feature at specific phases; and (4) a high level of excitation in their spectra, often including very strong He II λ4686 emission. A number of mechanisms have been proposed to explain the shared characteristics of this group, including (nondisk) circumstellar material around one or the other component (Smith et al. 1993), a bipolar wind from the disk (Honeycutt, Schlegel, & Kaitchuck 1986), and a strong (Williams 1989) or weak (Casares et al. 1996) white dwarf (WD) magnetic field, but none has been completely satisfying.

BH Lyncis (=PG 0818+513), along with DW Ursae Majoris (Shafter, Hessman, & Zhang 1988), V1315 Aquilae (Dhillon, Marsh, & Jones 1991), and the archetype SW Sextantis (Honeycutt et al. 1986), is among the handful of these systems that have undergone the closest scrutiny. BH Lyn was originally detected as a UV-excess object in the Palomar-Green photographic survey (Green, Schmidt, & Liebert 1986). Spectroscopic observations by Green et al. (1982) showed a high excitation emission-line spectrum indicative of an old nova. Andronov (1986) first noted the photometric variability of BH Lyn; an attempt by Richter (1989) to produce a composite light curve using magnitudes obtained from 15 archival plates taken hours to days apart yielded an unreliable orbital period of 0.577 day. Andronov et al. (1989) subsequently determined an orbital period of 0.15587490(2) day (≈3.74 hr) from 11 archival eclipse timings.

Dhillon et al. (1992, hereafter D92) obtained photometry and spectroscopy of BH Lyn in 1990 January. They added three new eclipse timings to the 11 of Andronov et al. (1989) to obtain a refined orbital period of 0.15587507(6) day. D92 also constructed Doppler tomograms (see § 3.9) of the Hβ, Hγ, Hδ, and He I λ4471 lines; however, these do not show much detail other than emission that is more or less centralized around the expected position of the WD. As noted by D92, the lack of significant ringlike structure in their tomograms does not support the presence of a prominent accretion disk in BH Lyn (or at least of an accretion disk that is a substantial emission source). Based on emission-line intensities compared to spectra obtained at a later date

[1] An exception to this "rule" is V795 Herculis ($P_{orb} = 2.6$ hr), which has recently been proposed as the first SW Sex star to be found *inside* the period gap (Casares et al. 1996).

(1991 April/May), they conclude that BH Lyn was in a low accretion rate state when they obtained the bulk of their spectra.

Thorstensen, Davis, & Ringwald (1991, hereafter T91) performed an in-depth study of BH Lyn as part of a program to measure orbital periods of CVs. Although published earlier, T91's data were obtained ~ 1 month after those of D92, in 1990 February. T91 found that the Hα emission-line equivalent width increases sharply during the eclipse ($\phi \approx 0.0$) and has a minimum half an orbit later ($\phi \approx 0.5$). Further, the Hα radial velocity curve shows a phase offset of $\Delta\phi \approx +0.16$; that is, the superior conjunction (red-to-blue crossing) of the Hα emission-line source occurs significantly later than the photometric eclipse (which is the assumed superior conjunction of the WD primary star). Such a phase offset is characteristic of the SW Sex stars. Although the spectroscopic results of T91 are somewhat different from those of D92, BH Lyn still seemed to be in a low state (characterized by a faint magnitude of $V \approx 17$).

We present new photometric and spectroscopic observations of BH Lyn, including the first *International Ultraviolet Explorer* (*IUE*) spectrum of this system. Unlike D92 and T91, our data were obtained during a high state of BH Lyn, as part of an ongoing campaign to investigate the accretion process in the SW Sex stars.

2. OBSERVATIONS

2.1. *Photometry*

We observed BH Lyn on 1995 October 22 UT with the 0.76 m telescope at the University of Washington's Manastash Ridge Observatory (MRO). The measurements were made through a V filter with the MRO 1024×1024 CCD detector. Each exposure was 180 s followed by 20–30 s of dead time to read out the CCD. A continuous series of exposures was made spanning 5.4 hr. Standard IRAF[2] tasks were used to perform overscan, bias, and flat-field corrections on each CCD image, and to obtain differential magnitudes for BH Lyn and two nearby stars of comparable brightness (C1 and C2). The uncertainty in the differential magnitudes was determined from the 1 σ deviation of the complete set of (C2 − C1) magnitudes, $\sigma = \pm 0.05$ mag.

In addition, we obtained sparsely sampled, two-color, broadband photometry of BH Lyn on 1994 November 18 UT and 1995 January 21 UT. These data sets are comprised of 5 s exposures used to check the slit positioning during our first two spectroscopy runs with the Double Imaging Spectrograph (DIS) on the Apache Point Observatory (APO) 3.5 m telescope (see § 2.2). The images were reduced with IRAF as described above; the same comparison stars were used as in the MRO data. The 1 σ deviations of the (C2 − C1) magnitudes are ± 0.05 mag in the "blue" and ± 0.07 mag in the "red."

2.2. *Spectroscopy*

We obtained three series of medium resolution (2 Å) optical spectra of BH Lyn using the DIS on the APO 3.5 m telescope, on 1994 November 18 UT, 1995 January 21 UT, and 1995 November 23 UT. Exposure times were 600 s in the 1995 November observations and 900 s on the other nights. After passing through a $6' \times 1''$ slit in the DIS, incoming starlight is split into two separately collimated beams by a dichroic with a transition wavelength of 5350 Å. Each beam then passes through a separate grating and falls onto a detector. The "blue" side utilizes an 830.8 line mm^{-1} grating with a thinned, UV-coated 512×512 SITe CCD; the "red" side utilizes a 1200 line mm^{-1} grating with a thinned 800×800 TI CCD. The grating tilts were set to give wavelength ranges of 4200–5000 Å on the blue side and 5800–6800 Å on the red side. The spectra were extracted and calibrated using standard IRAF routines (Massey, Valdes, & Barnes 1992); they were wavelength-calibrated via comparison with a He-Ne arc standard. Fine corrections to the wavelength calibration were made by examining the positions of night sky lines in the spectra. The wavelength scale of the blue spectra is accurate to ± 19 km s^{-1}, and that of the red spectra is accurate to ± 14 km s^{-1}. Both the blue and red spectra were flux-calibrated by using spectra of the standard stars Feige 34 and G191B2B obtained on each of the nights of observation.

On 1995 November 16 UT, we obtained two low-resolution (6 Å) ultraviolet (UV) spectra of BH Lyn using *IUE*. The short-wavelength (SWP) exposure was 180 minutes long and covers the wavelength range 1150–2000 Å; the long-wavelength (LWP) exposure was 60 minutes and covers 2000–3000 Å. The spectra were processed using the New Spectral Image Processing System (NEWSIPS) software.

3. RESULTS

3.1. *The Eclipse Ephemeris*

We observed two eclipses of BH Lyn on 1995 October 22 UT. The midpoint time of each eclipse was determined by fitting a parabola to the eclipse profiles, HJD(min) = 2,450,012.9062(23) and 2,450,013.0615(23). When compared to the ephemeris of D92, our eclipse timings have fairly large $O-C$ residuals of ≈ 0.0075 day and ≈ 0.0069 day, respectively. This continues the trend observed in the residuals of the D92 ephemeris: with the exception of the single Sonneberg timing (which has an anomalously large, positive residual) and the three Kishinev timings (which have a systematic negative offset in their $O-C$ values), the $O-C$ residual becomes increasingly positive at larger cycle numbers (see col. [3] of Table 1).

We derived an updated ephemeris for BH Lyn using our two mid-eclipse timings, the 11 timings in Andronov et al. (1989), the three timings in D92, plus an additional four timings obtained in 1989 by Chen, Wei, & Liu (1990):

$$\mathrm{HJD(min)} = 2,447,180.3368(2) + 0.15587520(5)E \; . \quad (1)$$

Each of the eclipse timings was weighted in inverse proportion to its reported uncertainty during the linear fitting process. The residuals for this ephemeris are listed in column (4) of Table 1. In general, they are smaller or comparable to the residuals obtained from the D92 ephemeris; most notably, our recent eclipse timings have significantly smaller residuals of ~ 0.025 in orbital phase. The residual for the oldest timing, obtained by Andronov et al. (1989) from the Sonneberg plate stack, is ~ 0.1 in orbital phase using our ephemeris. This point already had an unusually large residual from D92's ephemeris and does not follow the trend of the majority of the eclipse timings, plus it has a large uncertainty and so was weighted low in our fit. We

[2] The Image Reduction and Analysis Facility, v2.10.2, operated by the National Optical Astronomy Observatories.

TABLE 1

ECLIPSE OBSERVATIONS FOR BH LYNCIS

HJD at Mid-eclipse (2,400,000+) (1)	Cycle Number (epoch) (2)	D92 $O-C$ (days) (3)	Equation (1) $O-C$ (days) (4)	Equation (2) $O-C$ (days) (5)	Note (6)
38893.4036(47).....	−53164	+0.00892	+0.01697	+0.02464	1
45758.2873(15).....	−9123	−0.00134	+0.00013	+0.00161	2
47180.3363(7)	0	−0.00060	−0.00050	−0.00030	3
47180.4922(7)	1	−0.00058	−0.00048	−0.00028	3
47203.2505(3)	147	−0.00004	+0.00004	+0.00022	3
47203.4064(3)	148	−0.00001	+0.00007	+0.00025	3
47592.3150(6)	2643	+0.00029	−0.00001	−0.00018	3
47592.4709(6)	2644	+0.00032	+0.00002	−0.00015	3
47613.0480(23).....	2776	+0.00191	+0.00164	+0.00143	5
47613.2050(23).....	2777	+0.00303	+0.00277	+0.00255	5
47619.1260(23).....	2815	+0.00078	+0.00051	+0.00029	5
47619.2820(23).....	2816	+0.00090	+0.00064	+0.00041	5
47643.2843(8)	2970	−0.00156	−0.00190	−0.00212	4
47643.4402(8)	2971	−0.00153	−0.00188	−0.00209	4
47664.3275(14).....	3105	−0.00149	−0.00186	−0.00209	4
47904.5340(10).....	4646	+0.00152	+0.00093	+0.00048	6
47904.6912(10).....	4647	+0.00285	+0.00225	+0.00180	6
47909.5217(10).....	4678	+0.00122	+0.00062	+0.00017	6
50012.9062(23).....	18172	+0.00753	+0.00490	+0.00256	7
50013.0615(23).....	18173	+0.00695	+0.00433	+0.00198	7

NOTE.—The eclipse timings are given in: Andronov et al. 1989 from observations obtained in (1) Sonneberg, (2) Moscow, (3) Abastumani, and (4) Kishinev; (5) Chen at el. 1990; (6) D92; (7) this work.

suspect that the Sonneberg eclipse timing may be unreliable either due to human error or due to an actual long-term trend in the period of BH Lyn that cannot be reproduced with a linear ephemeris. So, we have derived a second ephemeris without this data point:

$$\mathrm{HJD(min)} = 2,447,180.3366(2) + 0.15587535(6)E\ . \quad (2)$$

In this case, the residuals of our recent eclipse timings are ~ 0.015 in orbital phase. The $O-C$ values for this ephemeris are listed in column (5) of Table 1. While equation (1) is the more technically correct ephemeris for BH Lyn because it includes all of the available eclipse timings, we will use equation (2) to phase our recently obtained spectra, since the latter ephemeris more accurately reproduces the times of eclipse from contemporary observations.

3.2. *The Light Curves*

The MRO V-band light curve of BH Lyn is shown in Figure 1. The eclipse is quite deep, $\Delta V \approx 1.5$ mag. Variability outside of eclipse in this light curve is much less pronounced than in those shown in D92 and Chen et al. (1990). There is little evidence of a pre-eclipse hump in the light curve caused by the changing aspect of a bright spot at the site where the accretion stream impacts the outer edge of the disk (as is seen in the light curves of many CVs, e.g., U Geminorum—Zhang & Robinson 1987).

Figure 2 shows the broadband light curves of BH Lyn obtained at APO on 1994 November 18 UT and 1995 January 21 UT and phased using the ephemeris of equation (2). While these light curves are sparsely sampled, the deep eclipse is visible in the November light curve and a pre-eclipse hump, with amplitude well in excess of the noise level determined from the comparison star light curves, is seen in the January light curve. The presence of a pre-eclipse hump in published light curves of BH Lyn ranges from nonexistent (Δ mag < 0.1; Andronov et al. 1989 and this work) to middling (Δ mag ~ 0.1–0.2; D92 and Chen et al. 1990) to strong (Δ mag $\gtrsim 0.3$; this work). While the presence of flickering with amplitude ~ 0.1 mag that is common in CV light curves can confuse this issue, a pre-eclipse hump is typically attributed to a bright spot located at the impact site of the accretion stream with the edge of the disk. If this is the case in BH Lyn, then the degree to which the stream impacts the edge of the disk may change over time.

Our comparison star C1 is one of the secondary standards calibrated by Henden & Honeycutt (1995). Their value of $V = 14.47$ for C1 corresponds to a mean magnitude for BH Lyn outside of eclipse (and excluding the pre-eclipse hump in the 1995 January light curve) of $V \approx 15.4$ in the MRO data and $V \approx 15.6$ in the APO data. Since the APO data were unfiltered, an additional correction factor was estimated by comparing the instrumental magnitudes of C1 in the APO light curves with its V magnitude in Henden & Honeycutt (1995). Consequently, the MRO magnitude is the more reliable value, but we estimate that the uncertainties in the two mean magnitudes are comparable

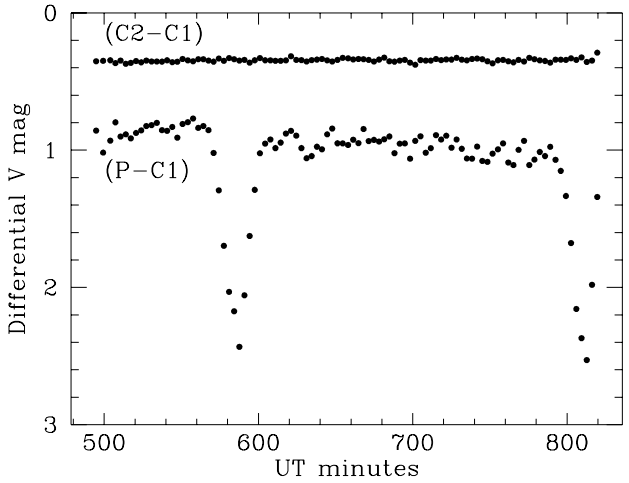

FIG. 1.—Light curve of BH Lyn in the V band obtained at MRO on 1995 October 22 UT.

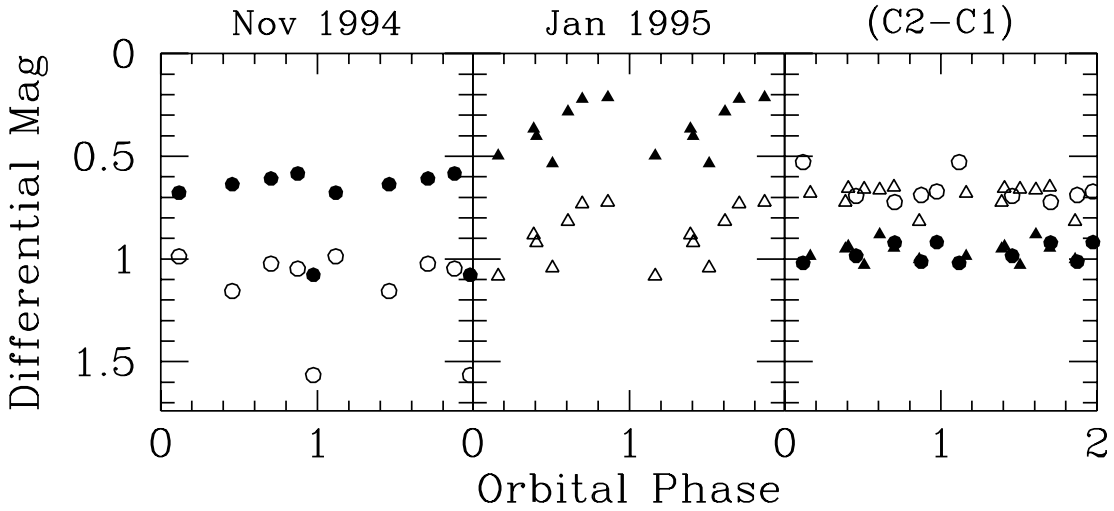

FIG. 2.—Light curves of BH Lyn from the DIS at APO on 1994 November 18 UT (*left*) and 1995 January 21 UT (*middle*). Filled symbols are from the "blue" side of DIS; open symbols are from the "red" side. The right panel shows the differential comparison star magnitudes used to estimate the noise level of the data. The data in all panels is repeated for clarity.

to their difference. In either case, these magnitudes are significantly brighter than the $V = 17.2 \pm 0.2$ found by D92 and the $V = 16.9 \pm 0.2$ found by T91, and show that BH Lyn was in a high state during our spectroscopic observations.

3.3. *The Optical Spectrum*

The orbital phase of each blue/red spectrum pair was calculated from the ephemeris of equation (2). There is significant variability of the low excitation line profiles at different orbital phases. Figure 3 shows the Hβ profile on the three nights of observation. This figure also shows the similarity of the lines from night to night despite the hump in the January light curve. In fact, the profile changes from orbit to orbit on the same night as much as it changes from night to night—the line profiles at phases 0.18 and 0.26 in the 1994 November data set are doubled because spectra at these phases were obtained on successive orbits; yet, they show substantial differences from each other. The spectra outside the range $\phi = 0.9$–0.1 in each of the November data sets were combined to give the average blue and red spectra shown in Figure 4. The average spectra are virtually identical from 1994 to 1995. Both show prominent emission lines of hydrogen and helium; He II λ4686 and the C III/N III complex near 4645 Å are especially strong when compared to the low state spectra of D92. The optical continua follow a power-law relation of $F_\lambda \propto \lambda^{-\alpha}$, where $\alpha \approx 1.9$. This is the same continuum flux distribution found by T91. By comparison, the theoretical spectrum of a steady state disk composed of particles radiating as blackbodies gives a power-law relation of $F_\lambda \propto \lambda^{-2.3}$ (Pringle 1981). This theoretical relation is consistent with the mean power-law slope of $\alpha = 2.3$ observed for a large sample of dwarf novae at outburst (Szkody 1985). However, as noted by T91, the somewhat flatter spectral distribution seen in BH Lyn is considered typical of nova-like CVs (Oke & Wade 1982).

3.4. *The Ultraviolet Spectrum*

The *IUE* spectrum of BH Lyn from Lyα to 2000 Å is shown in Figure 5. The unusually strong Al III λ1860 emission is due to contamination by a cosmic-ray hit. The other emission features in the UV spectrum of BH Lyn are similar to those seen in other nova-like CVs (including high inclination SW Sex stars such as DW UMa and SW Sex itself—see la Dous 1991). Equivalent widths of the emission lines indicated in Figure 5 are listed in Table 2. Each equivalent width was measured three times; the tabulated values are the means and standard deviations of the three trials for each line.

The origin of the "break" in the continuum near 1675 Å is not entirely clear. It may be related to the cosmic-ray hit near Al III, or it could be a manifestation of the "Fe II curtain" observed in the dwarf nova OY Carinae (Horne et al. 1994). The UV continuum from Lyα to 2900 Å follows a power law with index $\alpha \approx 0.2$; however, the continuum region from 2000 to 2900 Å has $\alpha \approx 1.7$, which is much steeper than over the entire *IUE* wavelength range and is comparable to the slope of the optical continuum. Similar steep UV continuum slopes are observed in high inclination dwarf novae during outburst when their mass accretion rates become large (e.g., Z Chamaeleontis, $\alpha \approx 1.6$–2.0; Harlaftis et al. 1992). This suggests that the continuum shortward of 2000 Å is being suppressed, possibly due to self-eclipse, or even disruption, of the hot inner disk.

3.5. *Radial Velocity Curves*

Radial velocities were measured from the wings of a number of emission lines in the BH Lyn optical spectra using the double Gaussian fitting technique described by

TABLE 2

ULTRAVIOLET EMISSION-LINE EQUIVALENT WIDTHS

Line	EW (Å)
N V λ1243	43.6(2.0)
Si III λ1294.....	24.4(2.2)
C II λ1335.....	37.0(4.4)
Si IV + O IV λ1400.....	210.0(7.9)
C IV λ1550.....	154.5(2.9)
He II λ1640	14.4(0.8)
N IV λ1718	32.8(1.6)

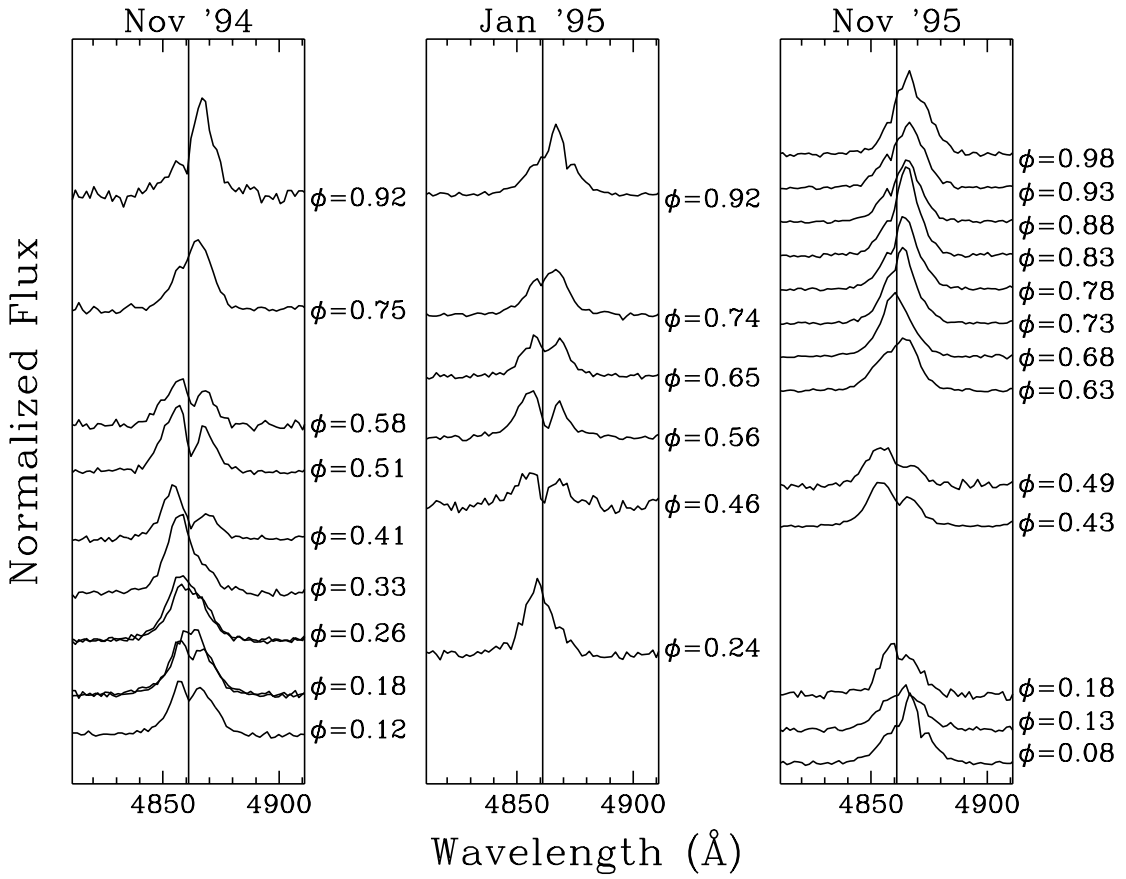

FIG. 3.—Emission-line profiles of Hβ in BH Lyn on the three nights of observation, showing the variations in profile shape from night to night and orbit to orbit (in the 1994 November data set).

Shafter, Szkody, & Thorstensen (1986) and Schneider & Young (1980). The FWHM of the Gaussians was set at 4 Å (i.e., twice the resolution of the spectra), and their separation a was varied from 10 to 54 Å for the prominent Balmer lines and from 10 to 42 Å for the weaker helium and metal lines. The equation

$$V(\phi, a) = \gamma(a) - K(a) \sin \{2\pi[\phi - \phi_0(a)]\} \quad (3)$$

was fitted to the velocity data obtained from the optimum value of the Gaussian separation. Because we combined data sets taken at substantially different times, the velocities from each set were shifted by the appropriate heliocentric correction prior to fitting. The best values (and 1 σ uncertainties as determined from Monte Carlo simulations) of the BH Lyn velocity parameters are listed in Table 3.

Note that the systemic velocity of the C III/N III complex is unreliable since an arbitrarily chosen central wavelength of 4645 Å was used in determining the velocity offsets. We have also included the radial velocity information from D92 and T91 to facilitate comparison with their low state observations.

Figure 6 shows the radial velocity data and best-fit sine curves for the six strongest lines. We had some concern that the spectra obtained in 1995 January would yield inconsistent results because of the presence of a prominent pre-eclipse hump in the January light curve. As seen in the figure, however, the January velocity points (*open triangles*) do not deviate significantly from the rest of the data, so we have used them in the fits. We suspect that the bright spot responsible for the pre-eclipse hump in the January light curve must be primarily a continuum source that does not greatly affect the profiles of the emission lines, especially in their high velocity wings. This assertion can be tested by comparing the phase-dependent behavior of the line and continuum fluxes in the 1995 January spectra. Some of our spectra may have suffered from slit losses and have unreliable absolute flux levels; however, we can plot a relative flux curve in terms of the fractional change from a median value. We have done this in the top panel of Figure 7 for the continuum, and Hβ and He II lines of the 1995 January

TABLE 3

EMISSION-LINE WING VELOCITY PARAMETERS

Line	a (Å)	K (km s^{-1})	γ (km s^{-1})	ϕ_0	$\sigma_{\rm TOTAL}$ (km s^{-1})
Hγ	26	129(10)	53(2)	0.17(1)	34
He I λ4471	18	127(10)	43(0)	0.11(1)	40
C III/N III	18	130(13)	147(4)	0.17(2)	54
He II λ4686	18	125(8)	77(2)	0.20(1)	28
Hβ	26	158(8)	54(1)	0.18(1)	29
He I λ4921	18	128(9)	26(4)	0.02(1)	42
He I λ5876	30	173(1)	−27(4)	0.19(1)	40
Hα	30	209(11)	49(3)	0.22(1)	42
He I λ6678	30	108(17)	52(5)	0.18(3)	74
from D92:					
Hδ		85(11)	53(8)	0.13(4)	
Hγ		103(8)	54(6)	0.11(3)	
He I λ4471		123(20)	51(12)	0.18(4)	
Hβ		118(8)	54(6)	0.13(2)	
from T91:					
Hα		191(13)	54(9)	0.16(2)	72

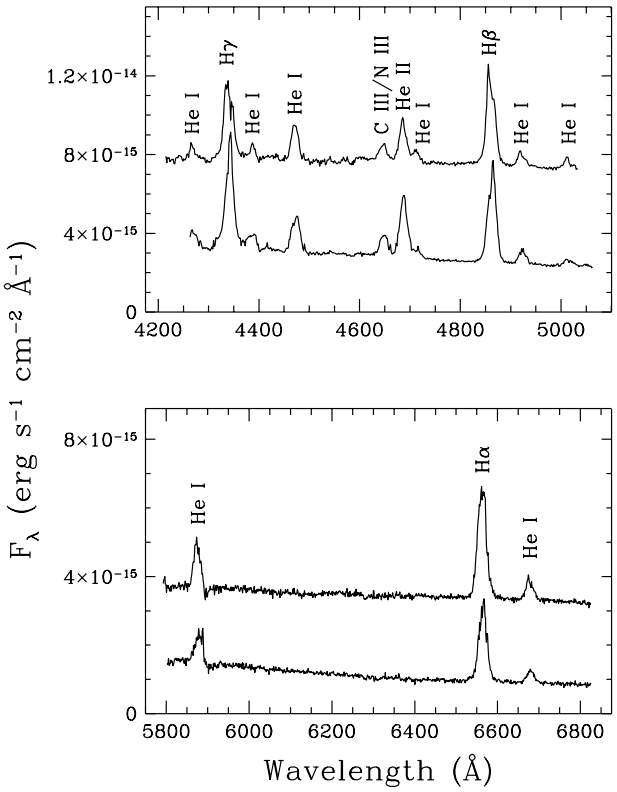

FIG. 4.—Average, out-of-eclipse optical spectrum of BH Lyn, uncorrected for orbital motion, obtained with the DIS on the APO 3.5 m telescope. The upper panel is from the "blue" side of DIS and the lower panel is from the "red" side. The upper spectrum in each panel is from 1994 November, while the lower spectrum is from 1995 November. The 1994 spectra have been shifted to higher flux for clarity, $F_\lambda + 5 \times 10^{-15}$ for the blue and $F_\lambda + 2 \times 10^{-15}$ for the red.

spectra. The continuum flux points are the means of the continuum levels at the central wavelength of each line; the line flux points are the total fluxes in the lines. The shapes of the three flux curves are identical to within about $\pm 10\%$ at each orbital phase and look very much like the APO light curve of BH Lyn from 1995 January (see Fig. 2). There is no significant change in the net fluxes of the emission lines due to the presence of the enhanced bright spot in the 1995 January data—they are simply superimposed on a brighter continuum.

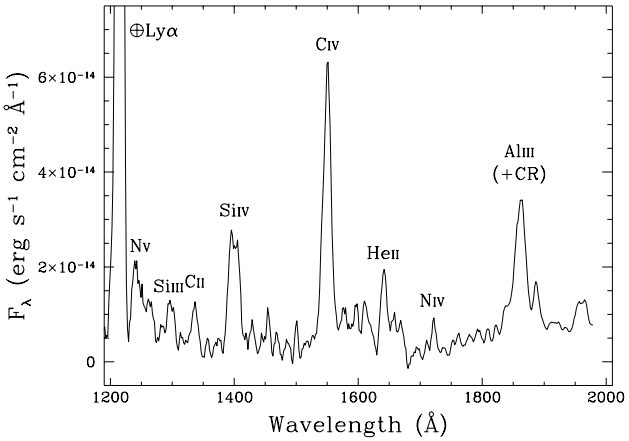

FIG. 5.—Short-wavelength UV spectrum of BH Lyn obtained with *IUE* on 1995 November 16 UT. The spectrum has been boxcar-smoothed by 3 pixels.

3.6. *System Parameters*

We calculated system parameters for BH Lyn using the method of Shafter (1984), Downes et al. (1986), and others, as described by Garnavich et al. (1990). We measured the full width at half-light of the eclipse from the MRO V-band light curve, $\Delta\phi_{1/2} = 0.079 \pm 0.015$, and used the velocity determined from the He II line, $K_{\rm WD} = 125 \pm 8$ km s^{-1}, as the WD orbital velocity.

It has been implicitly assumed that the secondary star in BH Lyn is a normal main-sequence star. This is probably not entirely the case, since the process of mass transfer will tend to force the secondary star out of thermal equilibrium and slightly above the main sequence. Fortunately, as noted by Garnavich et al. (1990), a change in the mass-radius relation for the secondary star translates into only a small shift in the mass ratio $q(=M_2/M_{\rm WD})$ and inclination i. The uncertainty in eclipse width has the largest effect on i, while the uncertainty in the WD orbital velocity has the largest effect on q. The best values of the system parameters in BH Lyn are: $i = 79(+5/-3)°$, $q = 0.45(+0.15/-0.10)$, $M_{\rm WD} = 0.73(+0.70/-0.36)\ M_\odot$, $M_2 = 0.33(+0.17/-0.11)\ M_\odot$, $R_2 = 0.38(+0.16/-0.12)\ R_\odot$, $a = 1.23(+0.63/-0.47)\ R_\odot$.

D92 calculated an inclination of $i = 80° \pm 5°$ and tentative mass ratio of $q \approx 0.4 \pm 0.3$. These estimates agree with our results, which is surprising since they were made from low state photometric light curves and Balmer line velocity curves, respectively. As can be seen from Table 3, however, D92's Balmer lines had much lower velocities ($K \approx 85$–118 km s^{-1}) than ours ($K \approx 129$–209 km s^{-1}); the orbital velocity used by D92 for the WD in BH Lyn is coincidentally comparable to the value we inferred from the He II line. Interestingly, T91's Hα radial velocity agrees with ours (within the uncertainties). This suggests that, despite the faint magnitude of BH Lyn during T91's observations, the CV was not in a pure low state (as in D92's observations) but was transitioning back to the high state.

Our upper limit on the WD mass exceeds the Chandrasekhar limit, which strongly implies that the mass ratio q is not likely to be at the low end of its range, while the orbital separation a and secondary star radius R_2 are not likely to be near the high ends of their ranges. As a final word of caution, these system parameters are only reliable in so far as it is true that the velocity curve of the He II emission line in BH Lyn is primarily governed by the motion of the WD. It is generally assumed to be the case in CVs that higher excitation emission lines originate closer to the WD and, hence, more accurately reflect its orbital motion (e.g., Shafter et al. 1988; Still, Dhillon, & Jones 1995). It is unclear, however, whether this maxim is applicable to BH Lyn, or to the SW Sex stars in general, considering that their line profiles have at least one peculiarity in being single-peaked rather than double-peaked. In the case of BH Lyn, the nonzero phase offset of the He II velocity solution implies that there may be contamination from nonorbital motion. Yet the velocity curves of the He II wing and peak components in BH Lyn (see §§ 3.5 and 3.7), the deep eclipse of He II relative to the Balmer lines (see § 4.1) and the He II Doppler tomogram (see § 3.9) suggest that this emission is indeed fairly centralized and located around the expected position of the WD, certainly more so than any of the lower excitation Balmer or He I lines. Thus, in the absence of

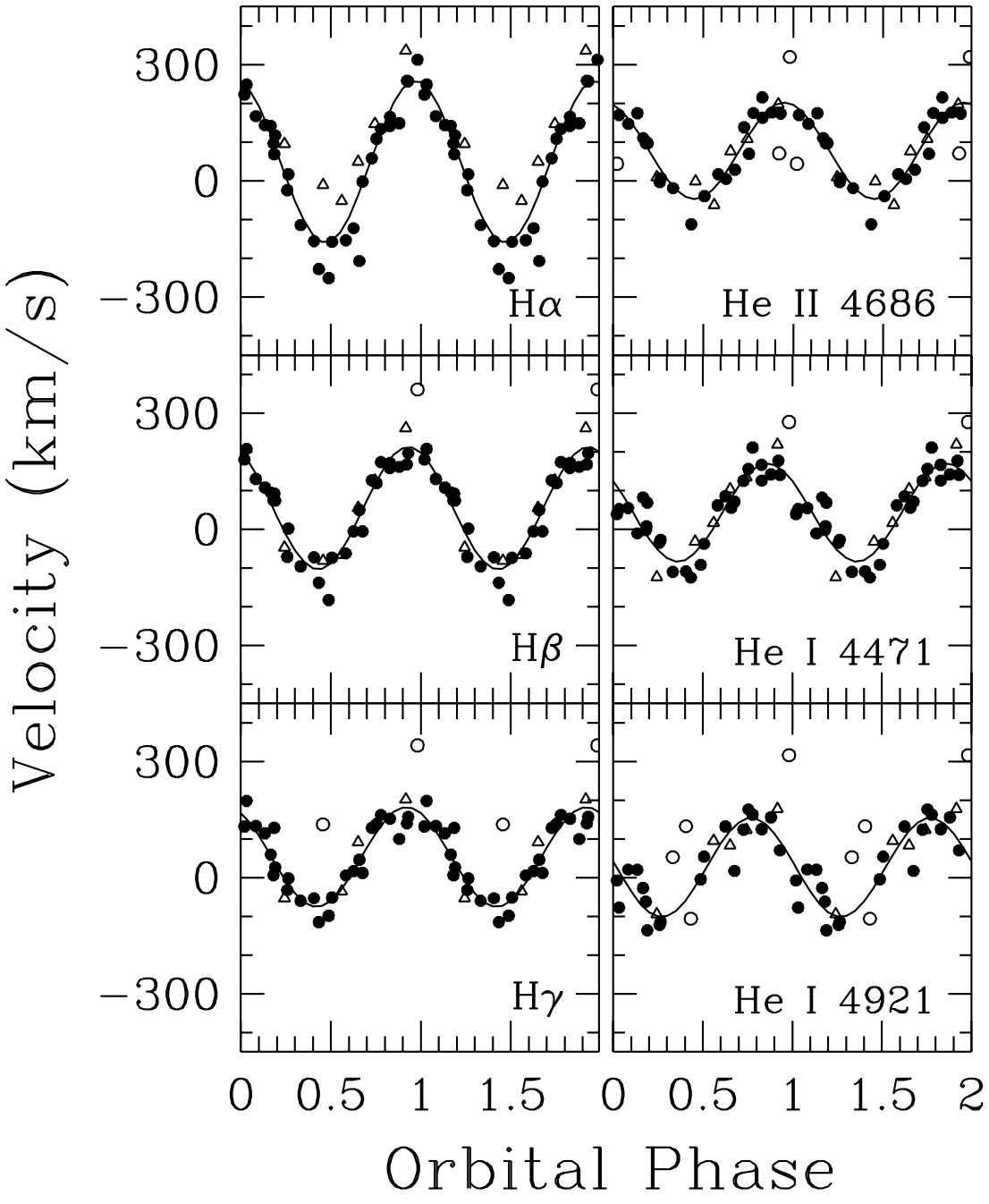

FIG. 6.—Emission-line radial velocities for BH Lyn, measured from the line wings using a double Gaussian fitting technique. The left panels show Hα (*top*), Hβ (*middle*), and Hγ (*bottom*); the right panels show He II λ4686 (*top*), He I λ4471 (*middle*), and He I λ4921 (*bottom*). The solid curves are the best-fit sine functions to the velocity data. Filled circles are data points from 1994 November and 1995 November; open circles were not used in the fit because they were either obtained during eclipse or during phases when contamination from the transient absorption feature was significant. The open triangles are points from 1995 January, when the light curve of BH Lyn displayed a prominent pre-eclipse hump. The January points were used in the fits because they do not show significant deviation from the 1994 and 1995 November data.

additional data, the He II line is currently the best means of arriving at an initial estimate of the WD orbital velocity and system parameters of BH Lyn.

3.7. *Velocities of Line Peaks*

In addition to measuring the radial velocities from the emission-line wings, the centroid of the peak in each line profile was determined. When more than one peak was visible in the line profile at a given phase (see Fig. 3), the velocity offset of the highest peak was measured. The velocity curves of the Balmer and He I peaks are shown in Figure 8. The solid line in each panel is the best fit of equation (3) to the data in that panel, while the dotted line is the best fit to the wing velocity data (from § 3.5) for the same line. Although there is somewhat more scatter in these plots than in the wing velocity curves, the 1995 January data (*squares*) do not deviate significantly from the curves followed by the other points. The bright spot causing the pre-eclipse hump in the 1995 January data must also contribute little or no flux to the central regions of the emission-line profiles. Table 4 lists the velocity parameters of the emission-line peaks (Balmer, He I, and also He II—see below). The 1 σ

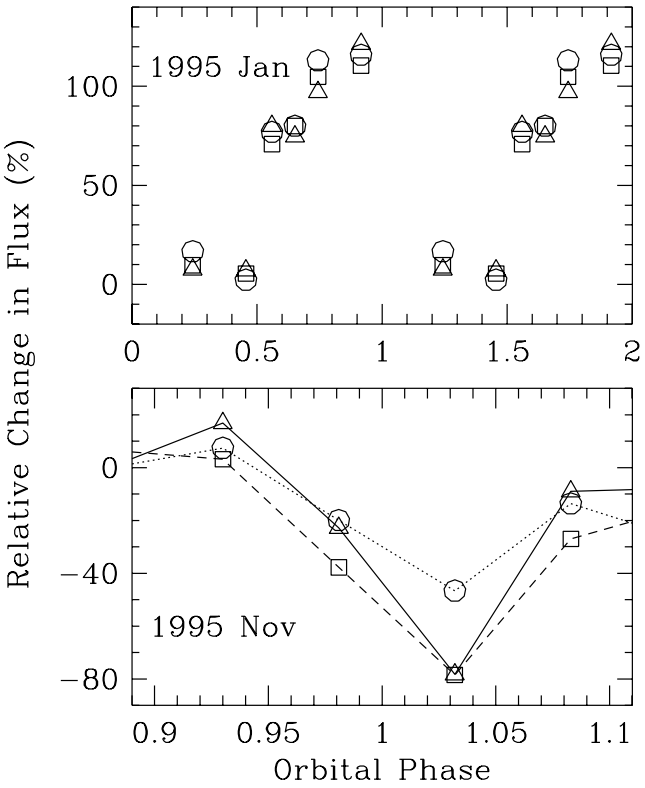

FIG. 7.—(*top*) The relative changes in flux of the Hβ emission lines (*circles*), the He II emission lines (*triangles*), and the continuum (squares) in the 1995 January spectra. (*bottom*) The relative changes in flux during the 1995 November eclipse of the Hβ (*circles*, *dotted line*) and He II (*triangles*, *solid line*) emission lines, and the continuum (*squares*, *dashed line*)—see § 4.1.

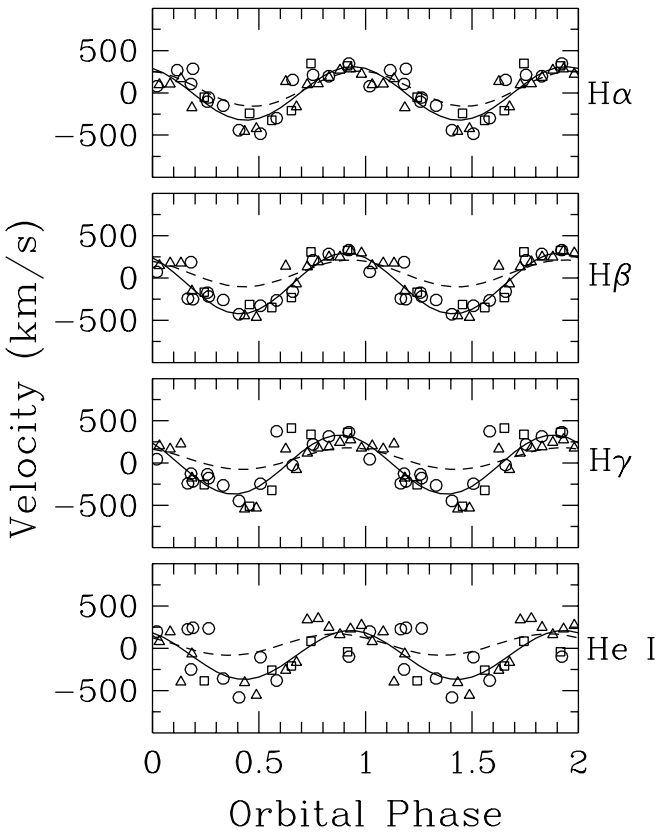

FIG. 8.—Velocity curves for the peak of the Hα, Hβ, Hγ, and He I λ4471 emission lines in BH Lyn. Circles are from 1994 November, squares are from 1995 January, and triangles are from 1995 November.

uncertainties were determined via Monte Carlo simulations around the best values, as in § 3.5.

The amplitudes of the peak velocity curves are larger than those of the corresponding wing curves: 288–360 km s^{-1} in the former case vs. 127–209 km s^{-1} in the latter case. Since the rotational velocity at all radii in the disk is larger than the orbital velocity of the secondary star (which, in turn, is larger than the orbital velocity of the primary star for $q < 1$), we interpret this to mean that the peak curve for a given line reflects the rotational motion of disk material passing through an emitting region that lies at a fixed position in the disk, while the wing curve for the same line shows the orbital motion of the emitting region around the center of mass of the system. The velocities of the Balmer and He I peaks undergo a blue to red crossing at $\phi \approx 0.65$; hence, this is the phase at which our line-of-sight is orthogonal to the motion of the primary emitting region in the disk. The source of this emission will be discussed in § 4.3.

TABLE 4

EMISSION-LINE PEAK VELOCITY PARAMETERS

Line	K (km s^{-1})	γ (km s^{-1})	ϕ_0	$\sigma_{\rm TOTAL}$ (km s^{-1})
Hγ.....	350(43)	−18(3)	0.12(2)	157
He I λ4471	288(61)	−79(5)	0.18(3)	203
He II λ4686.....	122(19)	35(1)	0.15(3)	71
Hβ	360(19)	−64(5)	0.16(1)	83
Hα	317(33)	−7(2)	0.19(2)	131

The velocity curve of the He II λ4686 peak is shown in Figure 9. Unlike the Balmer and He I lines, the He II line yielded a peak velocity curve quite similar to its wing velocity curve, with a phase offset of $\phi_0 = 0.15 \pm 0.03$ (vs. $\phi_0 = 0.20 \pm 0.01$ in the wings) and an amplitude of 122 ± 19 km s^{-1} (vs. 125 ± 8 km s^{-1} in the wings). The similarity in the velocity behavior of the wings and peak of He II suggests that only orbital motion is being observed; that is, the He II emitting region must be disconnected from the rotational field of the disk, originating either on the WD at the center of the disk or outside of the disk altogether (e.g., in a wind).

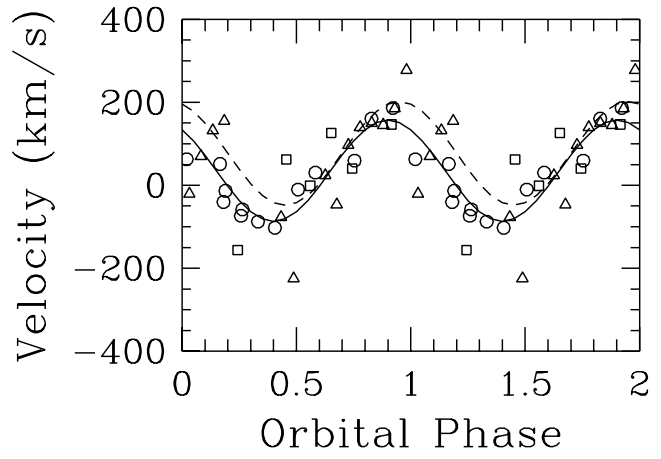

FIG. 9.—Velocity curve for the peak component of the He II λ4686 line in BH Lyn. Circles are from 1994 November, squares are from 1995 January, and triangles are from 1995 November.

3.8. *Equivalent Widths*

The equivalent widths of the emission lines were measured by direct integration of the pixel intensities between two manually selected endpoints. The equivalent width vs. orbital phase behavior of emission lines in BH Lyn is shown in Figure 10. The Balmer (but not He I) equivalent width curves contain a broad ($\Delta\phi \approx 0.3$), shallow ($\approx$10–15 Å) dip centered around $\phi \approx 0.5$ (see bottom left panel in Fig. 10). This dip was noted by T91 and is almost certainly produced by the prominent absorption feature in the Balmer (and He I) lines around $\phi = 0.5$. T91 also observed the very large peak in the Hα equivalent width near $\phi = 0.0$. The peak appears in our Hβ and Hγ equivalent widths as well, but at decreasing amplitude as we move up the Balmer series. It is also present with small amplitude in several He I lines

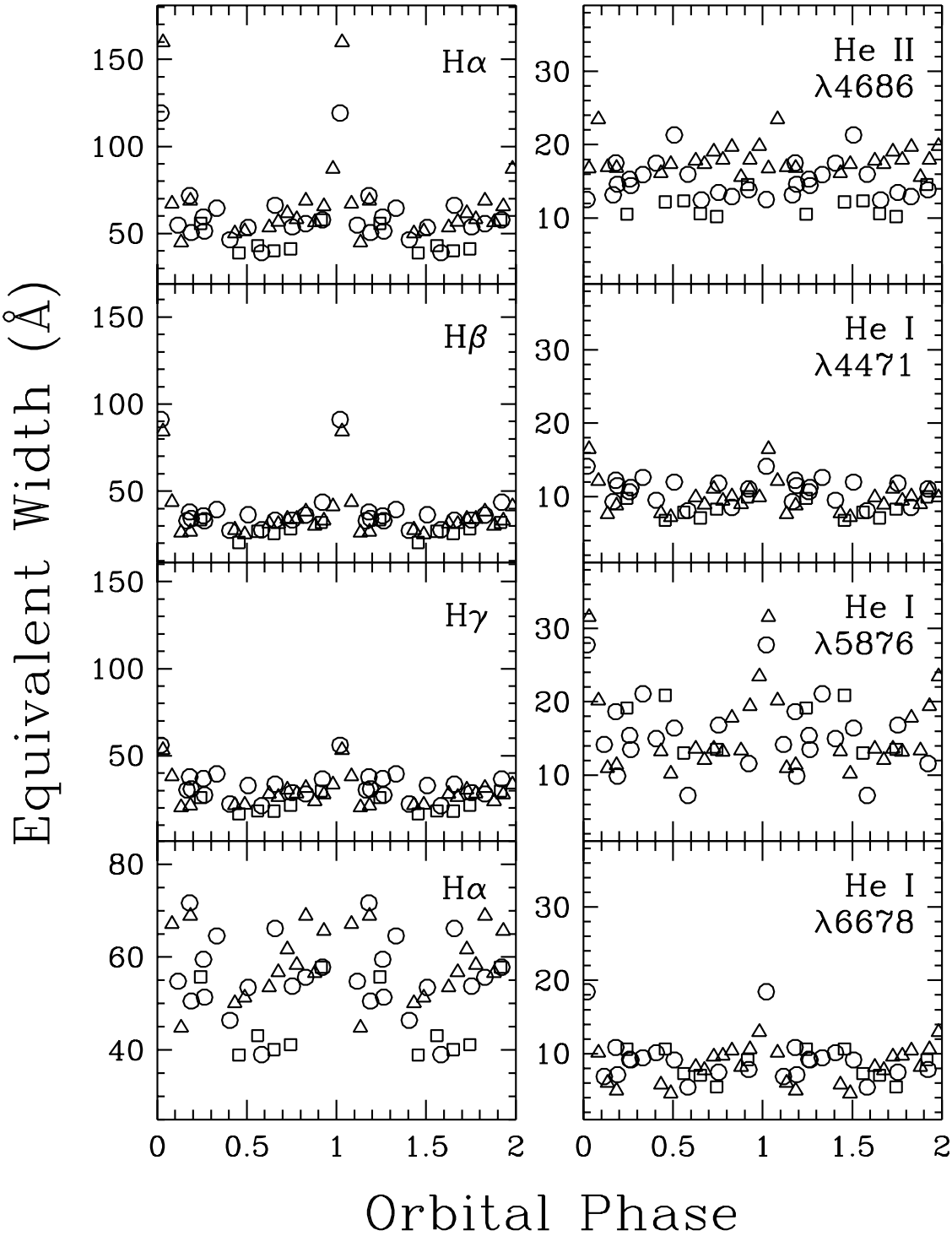

FIG. 10.—Equivalent widths of emission lines in BH Lyn plotted as a function of orbital phase (the data is repeated for clarity). The left panels show the Balmer lines; the top three panels have the same vertical scale, but the bottom panel redisplays the Hα data from the top panel on an expanded vertical scale to show the detail around $\phi \approx 0.5$. The right panels show the He II λ4686 line (*top*) and several He I lines. All of the panels have the same vertical scale. Circles are from 1994 November, squares are from 1995 January, and triangles are from 1995 November.

(λ4471, λ5876, λ6678) but is absent from the He II λ4686 line. This suggests that both the Balmer and He I emission lines are formed in a substantially different region than the He II line. In all of the equivalent width curves that display the peak, it is offset by $\Delta\phi \approx 0.03$ from $\phi = 0.0$. This appears to be a real, albeit small, shift—it is approximately twice the largest $O-C$ residual of contemporaneous eclipse timings from the ephemeris used to phase the spectra.

3.9. *Doppler Tomograms*

We have used the Fourier-filtered back-projection algorithm described by Horne (1991) and others (e.g., Marsh & Horne 1988; Kaitchuck et al. 1994) to produce Doppler tomograms of the velocity distribution of emitting material in BH Lyn. First, the individual spectra were rebinned into $\Delta\phi = 0.04$ intervals. Linear interpolation between spectra was used to "fill in" poorly sampled phase bins. Next, the spectra were arranged in order of phase to produce trailed spectrograms—the Hβ spectrogram is shown in Figure 11. These, in turn, were used to produce the Doppler tomograms. Spectra from orbital phases between 0.95 and 0.05 (i.e., the eclipse) were omitted from the tomography procedure. We constructed tomograms for six emission lines: Hγ, He I λ4471, He II λ4686, Hβ, He I λ5876, and Hα. They are shown in Figure 12 (Plate 15). For illustrative purposes we have plotted the Roche lobe of the secondary star, the expected trajectory of the accretion stream (*lower curve*), and the Keplerian velocities in the disk along the continuation of the stream trajectory (*upper curve*), based on the system parameters determined in § 3.6. Emission from the last of these positions is expected if the stream flows over its initial impact site and excites material in the disk along its path (Horne 1991).

The tomograms display several features of note:

1. The He II λ4686 tomogram shows a prominent central emission region surrounded by a roughly circular region of diffuse emission. The central region is slightly offset in the $-V_x$ direction from the $-V_y$ axis (along which the WD is located in velocity space), but its position is consistent with an origin on or near the WD.

2. The Balmer tomograms show prominent regions of intense emission located along the $-V_x$ axis. In the Hα tomogram, this region lies almost exactly on the $-V_x$ axis at $(V_x, V_y) \approx (-300, -50)$ km s^{-1}. This region moves to successively more negative V_y in progressing from Hα to Hβ ($V_y \approx -175$ km s^{-1}) to Hγ ($V_y \approx -250$ km s^{-1}). This suggests that there is a temperature stratification in the Balmer emission region.

3. The two He I lines (λ4471 and λ5876) are the weakest of the six lines for which tomograms were constructed and, consequently, yielded the noisiest tomograms. Even so, two primary emission regions are visible in these tomograms, one at approximately the same location as in the Hα tomogram and the other in the $(+V_x, -V_y)$ quadrant. The latter emission region probably "fills in" the He I equivalent width curves around $\phi = 0.5$ to mask the dip that is seen in the Balmer curves, but not in the He I curves.

4. In all of the tomograms, the positions of the secondary star's Roche lobe, the accretion stream, and the Keplerian continuation of the accretion stream do not coincide with strong emission. Nor is there strong emission in the velocity region between the two stream trajectories, where it might be expected due to the mixing of stream and disk material. Even if we consider the possible displacement of these locations due to the uncertainty in q, the primary emission regions in the tomograms still do not overlap them (see Fig. 13). The prominent emission regions in the Balmer tomo-

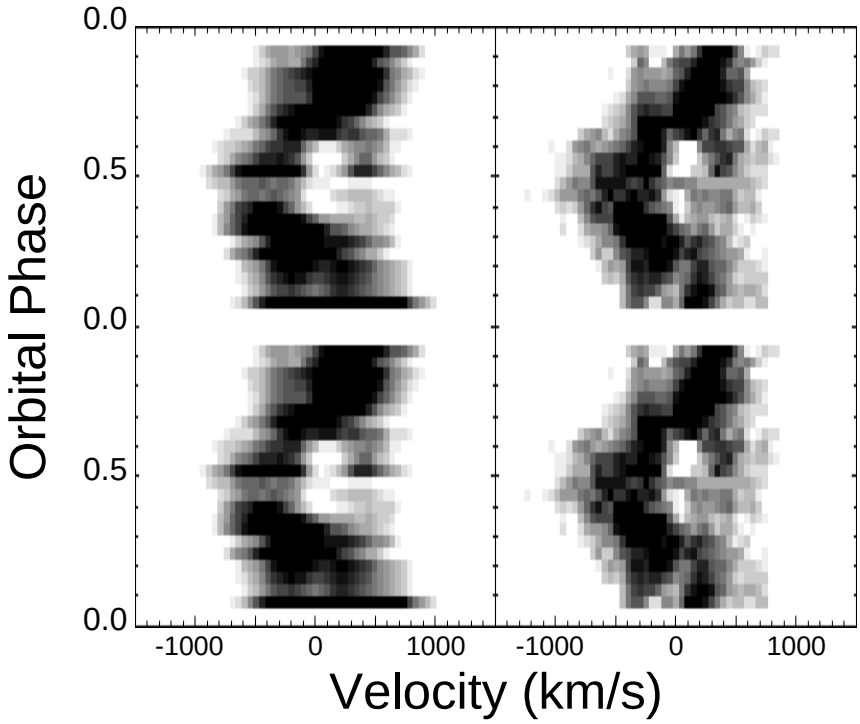

FIG. 11.—Left panel shows the trailed spectrogram for the Hβ emission line in BH Lyn. The right panel shows the predicted spectrogram produced by "forward-projecting" the Hβ tomogram constructed from the observed data. The gray-scale contrast in the spectrograms has been adjusted to emphasize the difference between emission (*black*) and absorption (*white*).

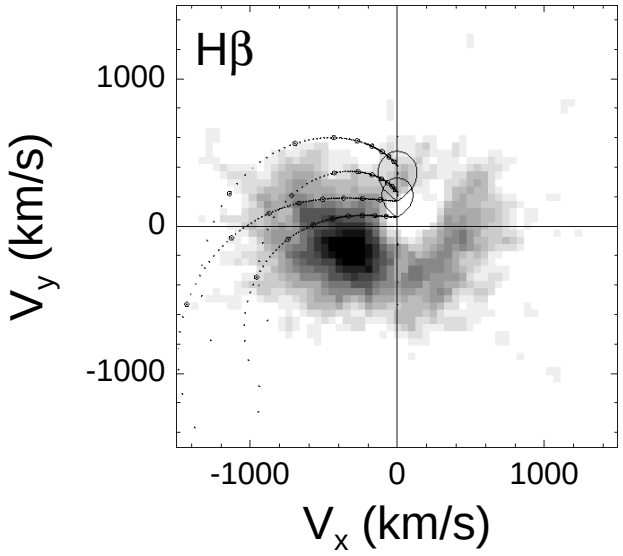

FIG. 13.—Hβ tomogram from Fig. 12 showing the secondary star Roche lobe and accretion stream paths for the maximum ($q = 0.6$; lower lobe) and minimum ($q = 0.35$; upper lobe) values of the mass ratio.

grams especially do not coincide with the expected position of the bright spot at the accretion stream impact site (which should be in the $(-V_x, +V_y)$ quadrant; e.g., see the Hβ tomograms of U Gem—a CV with a prominent bright spot—in Kaitchuck et al. 1994).

4. DISCUSSION

During the following discussion, it is prudent to keep in mind that the spectrum of a CV contains the spectrum of the *entire* binary system along a particular line of sight, and even emitting material at a relatively large vertical distance above the orbital plane of the binary will be represented in the emission-line profiles. The tomography process collapses the structure of the binary down to a two-dimensional plane defined by the inclination of the system. Thus, even if the source of a particular emission line is not confined to the accretion disk itself (e.g., if the emission originates in accretion columns that extend above the disk or in a wind emanating from the WD and/or disk face), the resultant tomogram still contains information about the structure of the system; however, its usefulness is limited by the lack of a one-to-one relation between position and velocity coordinates.

4.1. *The* He II *Line: Magnetic Channeling or Nonaxisymmetric Wind?*

In § 3.4, we mentioned the possibility that the inner regions of the disk in BH Lyn might be self-eclipsed or even missing altogether. Self-eclipse is certainly not an improbable occurrence in a high inclination system, and it is the simplest explanation for the depressed UV continuum in BH Lyn. There are two principal known methods for removing the inner disk in a CV, either through evaporation by a coronal siphon flow (Meyer & Meyer-Hofmeister 1994) or disruption by a WD magnetic field as in the intermediate polars (e.g., Patterson 1994). In the coronal siphon flow theory, evaporation of disk material forms a steady state, hot corona above the disk that accretes onto the WD. Additional material then evaporates off the disk to restore the equilibrium pressure in the corona, resulting in dissipation of the inner disk. Meyer & Meyer-Hofmeister (1994) note that the corona is only likely to be present during the quiescent state of dwarf novae. During outburst, the corona will be stripped away by a radiation-driven wind. They suggest that a similar case holds true for the nova-like CVs, whose steady high rate of mass transfer produces conditions similar to a constant dwarf nova outburst. Thus, while the prediction of a vertically extended corona or wind is of interest, it does not appear that the coronal siphon flow will work effectively in BH Lyn (or the other SW Sex stars).

Casares et al. (1996) have recently proposed a model for the SW Sex stars in which their unusual characteristics are the result of two accretion curtains/columns that extend from the inner edge of a magnetically disrupted disk to the magnetic poles of the WD. This model requires a class of transitionary magnetic CVs that contain both a partial disk (as in the DQ Her stars) *and* a WD with synchronized spin (as in the AM Her stars) but do not display characteristics of magnetic CVs such as strong X-ray emission and circularly polarized optical radiation. The latter requirement can be circumvented if the WD has magnetic field strength comparable to an AM Her star but the partial disk masks the polarized radiation, or if a WD with a magnetic field weaker than in an AM Her star can still synchronize without losing its disk. In hopes of explaining observations of the SW Sex star PX And, Still et al. (1995) performed a more quantitative examination of a similar magnetic model originally proposed by Williams (1989), but found it unconvincing. It is still possible, yet difficult to ascertain, that a magnetic field too weak to produce other observational characteristics could govern accretion close to the WD.

There has also been much discussion in the literature concerning the probable presence of a wind from the disk and/or WD in CVs (e.g., Vitello & Shlosman 1993; Piché & Szkody 1989; Honeycutt et al. 1986; Cordova & Mason 1985, and references therein). In the case of the SW Sex stars, a source of emission that is detached from the rotational (but not orbital) motion of the disk might account for the single-peaked emission lines. Hoare (1994) has modeled the line profiles expected for He II λ4686 emission from high inclination CVs and found good agreement with observed profiles. He predicts that both the continuum source and the He II emission region (at a distance of about $4R_{WD}$ above the disk) will be deeply eclipsed in a high inclination CV with similar system parameters to those we have determined for BH Lyn. The He II equivalent width curve of BH Lyn shows no evidence for any change during eclipse (nor does that of PX And—see Still et al. 1995). However, this does not necessarily mean that the He II emission is unaffected by the eclipse—an equal decrease in both the continuum and He II fluxes would maintain a constant equivalent width, as is the case in PX And. In the bottom panel of Figure 7, we have plotted relative flux curves (as described in § 3.5) for the continuum, and Hβ and He II emission lines at orbital phases around the eclipse in the 1995 November spectra. The depth of the He II eclipse is indeed approximately equal to that of the continuum eclipse, so that the He II equivalent width remains the same during eclipse. The Hβ eclipse, on the other hand, is much shallower than the continuum eclipse, thereby producing the large peak in Hβ equivalent width during eclipse.

If accretion onto the WD is magnetically governed, then preferential heating of one side of the WD due to channel-

ling of material onto its magnetic pole(s) could account for the small velocity offset of the He II emission. If the He II emission in BH Lyn originates in a wind, then the velocity offset of the emission region seen in the tomogram of that line may be the result of either shaping of the wind by nonaxisymmetric structure in the disk or of an intrinsically nonaxisymmetric wind produced, perhaps, by preferential accretion-induced heating of one side of the WD. The case for UV lines having their origins in a wind is much stronger than for their optical counterparts and significant phase lags ($\Delta\phi \approx 0.2$) observed in the UV lines of low inclination CVs can only be attributed to a wind origin if the outflow is nonaxisymmetric (Hoare 1994). An analogous argument may be applied to the optical lines of the SW Sex stars, which display phase lags of similar amplitude (e.g., $\Delta\phi \approx 0.15$–0.20 in BH Lyn). No matter what the exact origin of the He II line, the logical site for the source of such high excitation emission is on or near the WD.

4.2. *The Balmer and* He I *Lines: Further Evidence of Wind Emission?*

The large peak at $\phi \approx 0$ in the Balmer and He I equivalent widths in BH Lyn could be formed if the emission-line source is not as deeply eclipsed as the continuum, as in lines that form primarily in a low excitation corona or wind at a relatively large vertical distance from the disk. Along with his He II models, Hoare (1994) also performed preliminary simulations of Hβ emission from a wind but found that these models predict only a small contribution to the Balmer lines, plus an even smaller line forming region ($\approx 3R_{\rm WD}$) than for He II. He suggests that nonradial outflow from the disk could result in higher wind densities at greater distances, thereby yielding results that match observation.

T91 also observed a strong peak in the Hα equivalent width, but in D92's low state spectra the lines and continuum are both equally and totally eclipsed, and the eclipse depth increases at shorter wavelengths up the Balmer series (Table 5 compares several diagnostic features of BH Lyn in the low, intermediate, and high states).

The height of the peak in our equivalent width curves decreases in moving up the Balmer series, which is consistent with the pattern observed by D92. The small positive phase offset of the peak appears to rule out eclipse of the WD (which should occur at exactly $\phi = 0.0$) as the cause of the decreased continuum producing the peak. The phase offset of the peak is consistent with that expected for the eclipse of the bright spot at the accretion stream impact site (e.g., Robinson 1976; Wade 1981). If the bright spot is primarily a continuum source (as suggested in § 3.5), then its eclipse could be the cause of the peak in the Balmer and He I equivalent widths. Figure 7 shows that a continuum decrease of $\sim$40% more than the emission lines is required to account for the Hβ equivalent width peak in our 1995 November spectra. This would require the eclipse of a hump with a large amplitude of $\sim$0.35 mag, which is not observed in the 1994 and 1995 November data sets. If the bright spot is also a line-absorbing region, then its brightness could be substantially smaller while still producing the observed equivalent width effects. Unfortunately, we did not obtain a spectrum during eclipse in 1995 January, since it would be useful to see if the eclipse of a substantial bright spot has any effect on the equivalent width behavior of the emission lines.

4.3. *The $\phi \approx 0.5$ Absorption: Accretion Stream Overflow or Disk Bulges?*

Based on observations of the SW Sex star PX And and the gas dynamics calculations of Lubow (1989) and Lubow & Shu (1975), Hellier & Robinson (1994, hereafter H94) have suggested that the SW Sex phenomenon (in particular the $\phi \approx 0.5$ absorption) can be accounted for by absorption of the underlying disk emission as the accretion stream overflows its initial impact site at the disk edge and continues over the face of the disk to a secondary impact site. A number of shortcomings of this theory when compared to observational data have been pointed out by H94 and others. For example, the model predicts absorption of similar strength at opposite phase (Casares et al. 1996). This expectation is complicated by the eclipse, but the absorption feature lasts for $\Delta\phi \approx 0.2$–0.3 (Szkody & Piché 1990) vs. only $\Delta\phi \approx 0.1$ for the eclipse, and should still be observed. In general, this is not seen in any of the SW Sex stars. We note, however, that two of our line profiles of Hβ, at $\phi = 0.12$ and $\phi = 0.18$ (see Fig. 3), do appear to show some splitting reminiscent of the $\phi \approx 0.5$ absorption, albeit much shallower and less asymmetric. Also unlike the $\phi \approx 0.5$ absorption, this feature is not always present—the line profile of Hβ obtained an orbit earlier at $\phi = 0.18$ does not show the splitting, nor do any of the line profiles at similar phase in T91 and D92.

While overflow of the accretion stream is a common feature of numerical simulations of stream/disk interaction, Armitage & Livio (1996) have found in their three-dimensional smooth particle hydrodynamics (SPH) simulations of the stream and disk in interacting binaries that a well-collimated continuation of the stream is *not* formed. Instead, the impacting material forms a broad fan that is ejected to large distances (i.e., several times the disk scale height) above the plane of the disk. In different SPH simulations of accretion disks and streams, Meglicki, Wickramasinghe, & Bicknell (1993) noted the presence of a

TABLE 5

OBSERVATIONAL CHARACTERISTICS

Quality	High State[a]	Intermediate State[b]	Low State[c]
Brightness (V mag)	Bright ($\approx$15.5)	Faint (16.9)	Faint (17.2)
Balmer radial velocities (km s^{-1})	High ($\approx$129–209)	High ($\approx$191)	Low ($\approx$85–118)
Balmer equivalent width (Å)	Small ($\sim$50)	Large ($\sim$100)	Large ($\sim$100)
Balmer EW peak	Yes	Yes	No
He II λ4686 emission	Strong		Weak

[a] From this work.
[b] From T91.
[c] From D92.

substantial amount of turbulence in the interaction zone at the initial stream impact site. It is reasonable to assume, then, that the overflowing material, having gone through a forceful collision with the disk and subsequent ejection out of the orbital plane of the binary, will not carry its trajectory smoothly into the velocity field of the disk.

In the three-dimensional stream/disk simulations of Hirose, Osaki, & Mineshige (1991) and Meglicki et al. (1993) the resultant disks were found to develop "bulges" of varying thickness in the disk edge at phases of 0.2, 0.5, and 0.8 due to the buildup of impacting and overflowing material from the accretion stream. Hoard & Szkody (1996) utilized a model in which the $\phi = 0.8$ bulge dominates the disk structure to explain the behavior of PG 0859+415. They point out that this CV shares most of the other observational characteristics of the SW Sex stars, but the absorption feature appears in the emission lines at $\phi \approx 0.8$ rather than at $\phi \approx 0.5$ as in BH Lyn. They suggested that if the bulge at $\phi = 0.5$ were the dominant structure in the disk, then this might account for the absorption seen at $\phi \approx 0.5$ in the other SW Sex stars. This scenario has the advantage over absorption by the overflowing stream in that the bulge lies near the outer edge of the disk, so absorption of the intervening diffuse disk emission at the opposite phase is not expected to occur. In a recent refinement of the stream overflow model, Hellier (1996) concluded that while the model absorption from the overflowing stream reproduced the observed data adequately at other phases, it needed to be stronger at $\phi \approx 0.5$. He suggested a flared disk as a possible solution, but we note that the $\phi = 0.5$ bulge might also suffice.

Although a detailed quantitative examination of the effect of such a bulge on the observed properties of a CV is beyond the scope of this work, we can make some simple numerical estimates to test the plausibility of the bulge model. We assume that the emission region at $\phi \approx 0.65$ identified from the Balmer and He I peak velocity curves (see § 3.7) corresponds to the secondary impact site of the overflowing accretion stream and that the bulge begins at $\phi \approx 0.4$, extends to $\phi \approx 0.6$, and reaches a maximum height at $\phi \approx 0.5$. The large amplitudes of the peak velocity curves imply that the secondary impact site is located in the inner disk; hence, in order to absorb emission from that region, the bulge must be tall enough to obscure approximately from the edge of the disk to near its center as viewed at the inclination of the system,

$$H_{\rm bulge} \gtrsim R_{\rm disk} \sin (90^\circ - i) \approx 0.2 R_{\rm disk} . \quad (4)$$

This lower limit to the height of the bulge is only a factor of ≈ 2 larger than the expected height of the disk edge in a CV (e.g., Smak 1992), so it is not an unreasonable requirement.

The absorption around $\phi = 0.5$ is confined to a velocity range of ≈ -100 to $\approx +200$ km s^{-1} with the deepest absorption redward of both the emission peak and the rest velocity of the line center (see Fig. 11). A red offset of the absorption relative to the emission peak was also observed for the SW Sex stars DW UMa and SW Sex (Szkody & Piché 1990). In Figure 14, we have simulated the Hβ emission line from the secondary impact site, viewed at $\phi \approx 0.5$, as a Gaussian with an offset of -280 km s^{-1} (from the Hβ peak velocity curve) and a FWHM of 1100 km s^{-1} (the mean width of the Hβ line in the spectra of BH Lyn). The absorption from the bulge is simulated by an inverted Gaussian with zero offset (at $\phi \approx 0.5$ the bulge has approximately zero radial components of both orbital and disk-rotational velocities) and a width of ± 150 km s^{-1} (somewhat smaller than the expected range of rotational velocity at opposite sides of the disk—see § 3.7 and Frank, King, & Raine 1985). These two profiles were then added together to simulate the observed line profile. The depth of the bulge absorption was manually scaled to approximate the observed net absorption depth in the combined line. The absorption at the line center corresponds to an optical depth of ~ 1.3, which is consistent with the emission passing through a bulge with width ~ 0.05 of the disk radius (assuming $R_{\rm disk}$ is $\sim 70\%$ of the primary Roche lobe radius—Harrop-Allin & Warner 1996) and density comparable to assumed disk densities ($\rho \gtrsim 10^{13}$–10^{15} cm^{-3}; e.g., Warner 1976; Williams 1980; Livio, Soker, & Dgani 1986; Lin, Williams, & Stover 1988; Naylor et al. 1988). This simple simulation reproduces several important features of the observed line profiles. (1) The shape of the profile is similar to those at $\phi \approx 0.5$ in Figure 3. (2) The deepest absorption occurs between velocities of 0 and $+200$ km s^{-1}, as seen in the trailed spectrogram of the observed data. (3) As noted by Szkody & Piché (1990), the velocity of the absorption at phases before and after 0.5 can also be accounted for by a structure on the edge of the disk if there is additional absorption at $\phi \approx 0.4$ (as is provided by the overflowing accretion stream from H94's model).

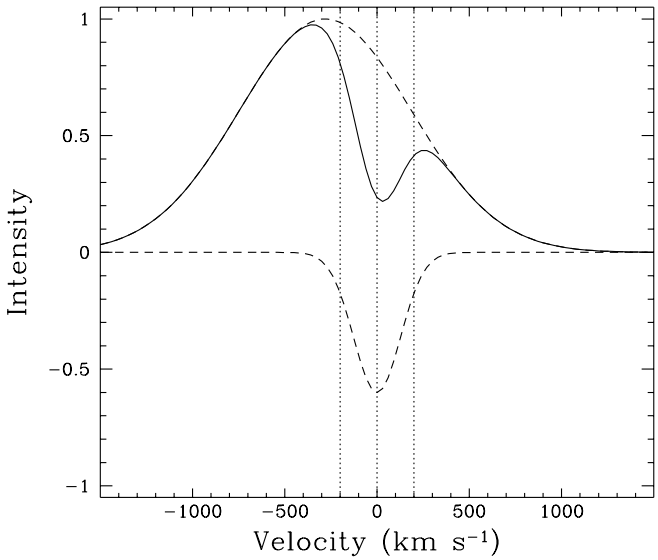

FIG. 14.—Simulated Hβ emission-line profile of BH Lyn viewed at $\phi \approx 0.5$. The emission from the secondary impact site of the overflowing accretion stream and the absorption from the bulge at the disk edge are represented by Gaussian functions (*dashed lines*). The solid line shows the combined line profile. The three vertical dotted lines are fiducials marking velocity offsets of -200, 0, and $+200$ km s^{-1}.

We believe the most plausible origin for the phase-dependent absorption feature in the SW Sex stars to be a combination of overflowing accretion stream and one of the bulges predicted in numerical simulations of stream/disk interaction. Although this model has now been applied to two SW Sex stars (BH Lyn and PG 0859+415) in order to account for their primary observational characteristics, it is not without a few problems. For example, the mechanism that would cause one of the bulges to dominate over the others is not entirely clear. Meglicki et al. (1993) and Hirose et al. (1991) performed similar simulations, and obtained

bulges at the same phases (0.2, 0.5, 0.8) in their resultant model disks, but a different one of the bulges had the maximum height in each case. The effect of small changes in system parameters (such as accretion rate, disk radius, etc.) on the relative sizes of the bulges has not been fully explored in the numerical simulations of stream/disk interaction. Also, although the presence of another bulge in the disk at $\phi = 0.2$ is predicted by the numerical simulations, it has so far remained undetected in observational data. It is not clear whether this is due to a shortcoming in the models or that the presence of a bulge on the "less energetic" side of the disk (i.e., away from the accretion stream, bright spot, and path of stream overflow) is simply below the threshold of detection. The tomograms of SW Sex stars often show less diffuse emission in the $(+V_x, +V_y)$ quadrant—between phases of 0.0 and 0.25—than in the other quadrants, which is suggestive of absorption between those phases. Certainly, the unambiguous detection of bulges in accretion disks at all three of the phases predicted by the models would give additional support to both the numerical models and the possibility that the bulges play an important role in producing the phase-dependent behavior of radiation emitted by the SW Sex stars and CVs in general.

We wish to thank Keith Horne for making his Doppler tomography software available to us, and Stefanie Wachter for reading a draft of this paper. This research was supported by NASA grant NAG-W-3158 and NSF grant AST9217911.

REFERENCES

Andronov, I. L. 1986, Astron. Tsirk., 1418
Andronov, I. L., Kimeridze, G. N., Richter, G. A., & Smykov, V. P. 1989, Inf Bull. Variable Stars, 3388
Armitage, P. J., & Livio, M. 1996, ApJ, 470, 1024
Beuermann, K., Thorstensen, J. R., Schwope, A. D., Ringwald, F. A., & Sahin, H. 1992, A&A, 256, 442
Casares, J., Martínez-Pais, I. G., Marsh, T. R., Charles, P. A., & Lázaro, C. 1996, MNRAS, 278, 219
Chen, J.-S., Wei, M.-Z., & Liu, X.-W. 1990, Acta Astron. Sin., 31, 305
Cordova, F. A., & Mason, K. O. 1985, ApJ, 290, 671
Dhillon, V. S., Jones, D. H. P., Marsh, T. R., & Smith, R. C. 1992, MNRAS, 258, 225 (D92)
Dhillon, V. S., Marsh, T. R., & Jones, D. H. P. 1991, MNRAS, 252, 342
Downes, R. A., Mateo, M., Szkody, P., Jemmer, D. C., & Margon, B. 1986, ApJ, 301, 240
Frank, J., King, A. R., & Raine, D. J. 1985, in Accretion Power in Astrophysics (Cambridge: Cambridge Univ. Press)
Garnavich, P. M., et al. 1990, ApJ, 365, 696
Green, R. F., Ferguson, D. H., Liebert, J., & Schmidt, M. 1982, PASP, 94, 560
Green, R. F., Schmidt, M., & Liebert, J. 1986, ApJS, 61, 305
Harlaftis, E. T., Naylor, T., Hassall, B. J. M., Charles, P. A., Sonneborn, G., & Bailey, J. 1992, MNRAS, 259, 593
Harrop-Allin, M. K., & Warner, B. 1996, MNRAS, 279, 219
Hellier, C. 1996, ApJ, 471, 949
Hellier, C., & Robinson, E. L. 1994, ApJ, 431, L107 (H94)
Henden, A. A., & Honeycutt, R. K. 1995, PASP, 107, 324
Hirose, M., Osaki, Y., & Mineshige, S. 1991, PASJ, 43, 809
Hoard, D. W., & Szkody, P. 1996, ApJ, 470, 1052
Hoare, M. G. 1994, MNRAS, 267, 153
Honeycutt, R. K., Schlegel, E. M., & Kaitchuck, R. H. 1986, ApJ, 302, 388
Horne, K. 1991, in Fundamental Properties of Cataclysmic Variable Stars: Proc. 12th North American Workshop on Cataclysmic Variables and Low Mass X-Ray Binaries, ed. A. W. Shafter (San Diego: San Diego State Univ.), 23
Horne, K., Marsh, T. R., Cheng, F. H., Hubeny, I., & Lanz, T. 1994, ApJ, 426, 294
Kaitchuck, R. H., Schlegel, E. M., Honeycutt, R. H., Horne, K., Marsh, T. R., White, J. C. II, & Mansperger, C. S. 1994, ApJS, 93, 519
la Dous, C. 1991, A&A, 252, 100
Lin, D. N., Williams, R. E., & Stover, R. J. 1988, ApJ, 327, 234
Livio, M., Soker, N., & Dgani, R. 1986, 305, 267
Lubow, S. H. 1989, ApJ, 340, 1064
Lubow, S. H., & Shu, F. H. 1975, ApJ, 198, 383
Marsh, T. R., & Horne, K. 1988, MNRAS, 235, 269
Massey, P., Valdes, F., & Barnes, J. 1992, A User's Guide to Reducing Slit Spectra with IRAF, available on-line at http://iraf.noao.edu/
Meglicki, Z., Wickramasinghe, D., & Bicknell, G. V. 1993, MNRAS, 264, 691
Meyer, F., & Meyer-Hofmeister, E. 1994, A&A, 288, 175
Naylor, T., Charles, P. A., Drew, J. E., & Hassall, B. J. M. 1988, MNRAS, 233, 285
Oke, J. B., & Wade, R. A. 1982, AJ, 87, 670
Patterson, J. 1994, PASP, 106, 209
Piché, F., & Szkody, P. 1989, AJ, 98, 2225
Pringle, J. E. 1981, ARA&A, 19, 137
Richter, G. A. 1989, Inf. Bull. Variable Stars, 3287
Robinson, E. L. 1976, ARA&A, 14, 119
Schneider, D. P., & Young, P. 1980, ApJ, 238, 946
Shafter, A. W. 1984, AJ, 89, 1555
———. 1992, ApJ, 394, 268
Shafter, A. W., Hessman, F. V., & Zhang, E.-H. 1988, ApJ, 327, 248
Shafter, A. W., Szkody, P., & Thorstensen, J. R. 1986, ApJ, 308, 765
Smak, J. 1992, Acta Astron., 42, 323
Smith, R. C., Fiddik, R. J., Hawkins, N. A., & Catalan, M. S. 1993, MNRAS, 264, 619
Still, M. D., Dhillon, V. S., & Jones, D. H. P. 1995, MNRAS, 273, 863
Szkody, P. 1985, in Recent Results on Cataclysmic Variables: Proc. ESA Workshop, ed. W. R. Burke (Bamberg: ESA SP-236), 39
Szkody, P., & Piché, F. 1990, ApJ, 361, 235
Thorstensen, J. R., Davis, M. K., & Ringwald, F. A. 1991, AJ, 102, 683 (T91)
Vitello, P., & Shlosman, I. 1993, ApJ, 410, 815
Wade, R. A. 1981, ApJ, 246, 215
Warner, B. 1976, in Structure and Evolution of Close Binary Systems, ed. P. Eggleton, S. Mitton, & J. Whelen (Dordrecht: Reidel), 85
Williams, R. E. 1980, ApJ, 235, 939
———. 1989, AJ, 97, 1752
Zhang, E.-H., & Robinson, E. L. 1987, ApJ, 321, 813

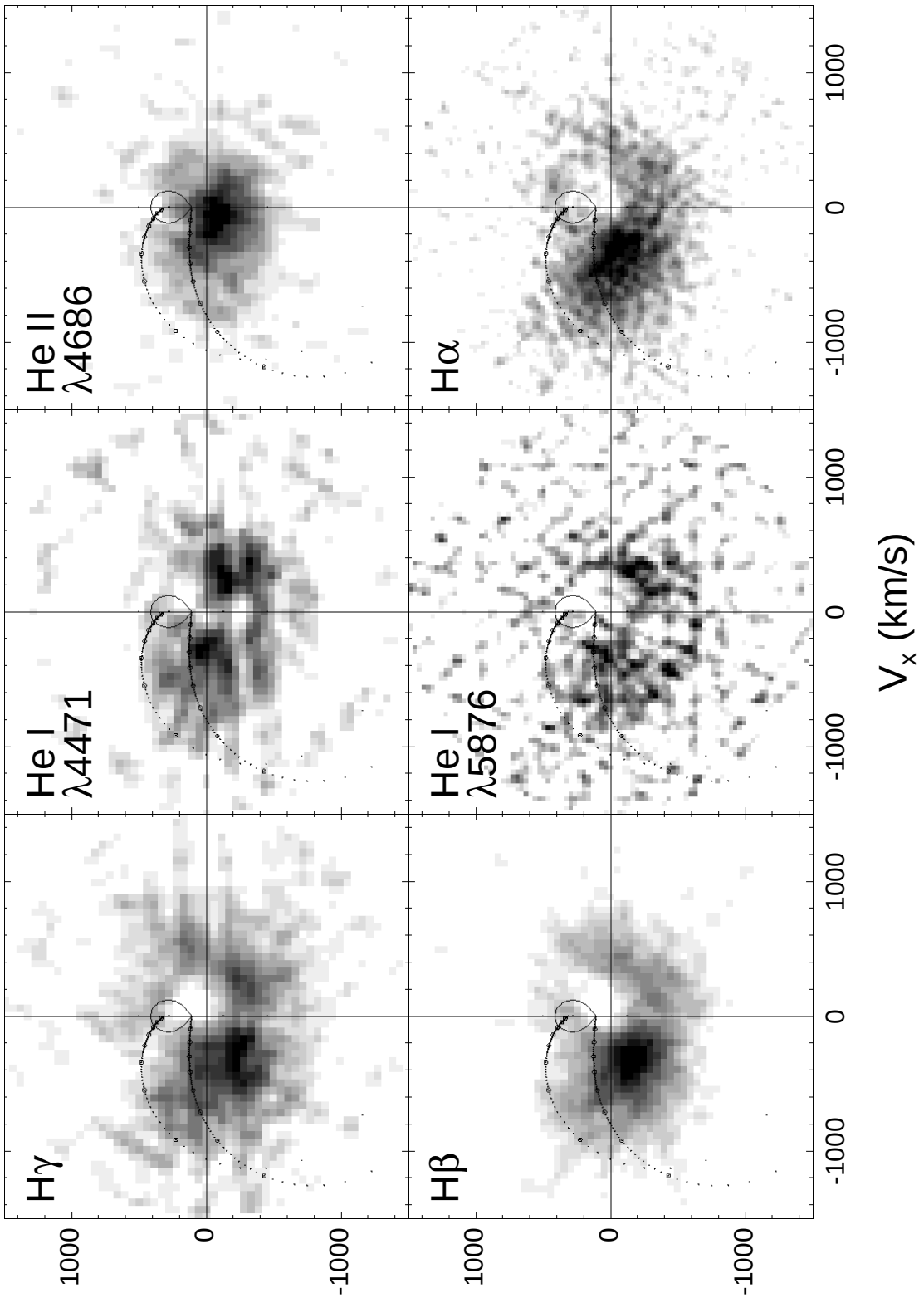

FIG. 12.—Doppler tomograms for six emission lines of BH Lyn. The images are displayed in a reverse gray scale so that emission regions are dark. The positions of the Roche lobe of the secondary star, the expected trajectory of the accretion stream (*lower curve*), and the Keplerian velocities in the disk along the continuation of the stream trajectory (*upper curve*)—based on our system parameters for BH Lyn—are plotted in the tomograms.